Structural Details of the Thermophilic Filamentous Bacteriophage PH75 Determined by Polarized Raman Microspectroscopy†

Masamichi Tsuboi, James M. Benevides, Priya Bondre, and George J. Thomas, Jr.*

Division of Cell Biology and Biophysics, School of Biological Sciences, University of Missouri−Kansas City, 5100 Rockhill Road, Kansas City, Missouri 64110

Received September 23, 2004; Revised Manuscript Received January 14, 2005

ABSTRACT: The filamentous virus PH75, which infects the thermophile *Thermus thermophilus*, consists of a closed DNA strand of 6500 nucleotides encapsidated by 2700 copies of a 46-residue coat subunit (pVIII). The PH75 virion is similar in composition to filamentous viruses infecting mesophilic bacteria but is distinguished by in vivo assembly at 70 °C and thermostability to at least 90 °C. Structural details of the PH75 assembly are not known, although a fiber X-ray diffraction based model suggests that capsid subunits are highly α-helical and organized with the same symmetry (class II) as in the mesophilic filamentous phages Pf1 and Pf3 [Pederson et al. (2001) *J. Mol. Biol. 309,* 401−421]. This is distinct from the symmetry (class I) of phages fd and M13. We have employed polarized Raman microspectroscopy to obtain further details of PH75 architecture. The spectra are interpreted in combination with known Raman tensors for modes of the pVIII main chain (amide I) and Trp and Tyr side chains to reveal the following structural features of PH75: (i) The average pVIII peptide group is oriented with greater displacement from the virion axis than peptide groups of fd, Pf1, or Pf3. The data correspond to an average helix tilt angle of 25° in PH75 vs 16° in fd, Pf1, and Pf3. (ii) The indolyl ring of Trp 37 in PH75 projects nearly equatorially from the subunit α-helix axis, in contrast to the more axial orientations for Trp 26 of fd and Trp 38 of Pf3. (iii) The phenolic rings of Tyr 15 and Tyr 39 project along the subunit helix axis, and one phenoxyl engages in hydrogen-bonding interaction that has no counterpart in either fd or Pf1 tyrosines. Also, in contrast to fd, Pf1, and Pf3, the packaged DNA genome of PH75 exhibits no Raman anisotropy, suggesting that DNA bases are not oriented unidirectionally within the nucleocapsid assembly. The structural findings are discussed in relation to intrasubunit and intersubunit interactions that may confer hyperthermostability to the PH75 virion. A refined molecular model is proposed for the PH75 capsid subunit.

Filamentous bacteriophage PH75, which infects the thermophilic bacterium *Thermus thermophilus*, comprises a covalently closed DNA single strand (ss)[1] of approximately 6500 nucleotides that is encapsidated by ∼2700 copies of a 46-residue major coat protein subunit (∼2.4 nucleotides per subunit), plus several copies of a few minor proteins located at the filament ends. The structure of PH75 has been investigated recently by methods of fiber X-ray diffraction (*1*), Raman optical activity (ROA) (*2*), and solution Raman spectroscopy (*3*). The overall morphology (flexible rod) and dimensions of the virion (∼6 × 910 nm) resemble those of the much studied mesophilic filamentous phages, fd, Pf1, and Pf3 (*4*, *5*). Nevertheless, distinct structural features are evident for each member of the filamentous phage family. For example, the major capsid subunit of PH75 (sequence: MDFNPSEVAS^{10}QVTNYIQAIA^{20}AAGVGVLALA^{30}-IGLSAAWKYA^{40}KRFLKG^{46}) manifests no sequence homology with coat proteins of other filamentous phages, even though all comprise three distinct domains, namely, a polar and acidic N-terminal region located at the capsid exterior (residues 1−17 for PH75), a hydrophobic central region forming the intersubunit surface (18−33), and a basic C-terminal region lining the capsid interior and adjoining the packaged ssDNA (37−46). PH75 is also distinguished from fd, Pf3, and Pf1 by virtue of in vivo assembly at 70 °C.

On the basis of fiber X-ray diffraction experiments exhibiting meridional and equatorial resolutions of 2.4 and 3.1 Å, respectively, a molecular model has been proposed for the PH75 capsid (*1*). However, the conformations and interactions of coat protein side chains in the capsid are not revealed directly by the fiber diffraction data, and their elucidation requires alternative biophysical approaches. To obtain such detailed structural information on large biomolecular assemblies, we have developed appropriate methods of polarized Raman spectroscopy. Our approach exploits the use of a Raman microscope to measure Raman scattering anisotropies from oriented specimens and the interpretation of the polarized Raman spectral data in conjunction with known Raman tensors (*6*).

Typically, the Raman spectrum of an oriented fiber of a filamentous bacteriophage consists of about 50 prominent

† Part LXXXVI in the series Structural Studies of Viruses by Raman Spectroscopy. Supported by NIH Grant GM50776.

* To whom correspondence should be addressed. E-mail: thomasgj@umkc.edu. Telephone: 816-235-5247. Fax: 816-235-1503.

[1] Abbreviations: ss, single strand; ROA, Raman optical activity; Tris, tris(hydroxymethyl)aminoethane.

10.1021/bi0479306 CCC: $30.25
Published on Web 03/02/2005

bands in the 200−1800 cm^{-1} spectral interval. The Raman scattering intensity of each band depends on the directions of the electric vectors of the incident and Raman scattered light, as well as upon the associated Raman tensor of the molecular vibration giving rise to the band. If the Raman tensor of a particular vibration is known, i.e., if the axes of orientation of the principal components of the Raman tensor (α_{xx}, α_{yy}, α_{zz}) are known in relation to the geometry of the vibrating molecular group, then appropriate polarized Raman measurements on an oriented sample can be used to establish the orientation of the molecular group (*6*). Using this approach for the Raman amide I band, we have determined the average orientation of the coat protein α-helices in each of the filamentous viruses fd, Pf1, and Pf3 (*7*−*9*). We have also used this approach with Raman bands of the tryptophan and tyrosine side chains to determine the orientations of these moieties in the same filamentous virus assemblies (*8*−*11*).

Here, we report a polarized Raman microspectroscopic determination of the orientations of the coat protein α-helix and tryptophan (Trp 37) and tyrosine (Tyr 15 and Tyr 39) side chains in the PH75 virion. In separate publications, we have reported the basis for the relevant PH75 Raman band assignments (*3*) and the associated Raman tensor determinations (*6*, *12*−*14*). Although the present results reveal some structural similarities between PH75 and the mesophilic phages, the PH75 virion exhibits a unique set of side chain orientations and architectural details. These distinctive features are discussed in relation to the thermophilic character of bacteriophage PH75.

MATERIALS AND METHODS

Sample Preparation. PH75 was grown in *T. thermophilus* strain HB8 using stocks obtained from Dr. Michael Slater, Promega Corp., Madison, WI. The growth medium contained, per liter, 3 g of tryptone, 3 g of yeast extract, 5 g of disodium succinate, 0.7 g of $NaNO_3$, 0.1 g of $CaCl_2 \cdot 2H_2O$, 0.1 g of KNO_3, 0.1 g of $MgCl_2 \cdot 7H_2O$, 2.9 mg of boric acid, 1.8 mg of $MnCl_2 \cdot 4H_2O$, 0.25 mg of $ZnSO_4 \cdot 7H_2O$, 0.1 mg of $CuSO_4 \cdot 5H_2O$, 0.1 mg of $CoCl_3 \cdot 6H_2O$, and 0.4 mg of $Na_2MoO_4 \cdot 2H_2O$. The pH of the medium was adjusted to 8.3 with concentrated NaOH solution. An aliquot (100 μL) of late-log culture was used to inoculate the heated growth medium (400 mL, 70 °C), which was infected with PH75 at a multiplicity of infection of 100 and incubated for about 16 h. After centrifugation at 6000*g*, each 400 mL of cooled supernatant was treated with 16 g of NaCl and 24 g of PEG, stirred at 4 °C for 24 h, and centrifuged at 15000*g*. The resulting phage pellet was resuspended in 5 mL of 5 mM Tris, pH 7.5, and separated as a homogeneous band on a CsCl gradient. The band was removed, dialyzed once against 5 mM Tris containing 0.5 M NaCl and three times against 5 mM Tris, and finally brought to a concentration of ∼10 mg/mL in 5 mM Tris, pH 7.5, for storage at 4 °C. Typically, a 400 mL preparation yielded 30−40 mg of purified PH75 phage. Further details of the growth, purification, and titering procedures have been described (*1*).

Oriented PH75 fibers of ∼0.5 mm thickness were prepared for polarized Raman spectroscopy by slowly drawing a droplet of PH75 solution (∼100 mg/mL in 10 mM Tris, pH 7.8) in a fiber pulling device maintained at 20 °C and 92% relative humidity (*7*). The oriented fiber was sealed in a hygrostatic chamber and placed on the microscope stage for subsequent polarized Raman measurements. Optimally aligned samples contained between 95% and 100% of the PH75 particles oriented unidirectionally (*7*).

Raman Microspectroscopy. Raman spectra were recorded on a Jobin-Yvon Labram Infinity Micro Raman spectrophotometer (Jobin-Yvon Inc., Horiba Group, Edison, NJ) using 532 nm excitation from a Millennium-V Nd:YVO_4 laser (Spectra Physics, Mountain View, CA) maintained at 200 mW at the laser head. The laser beam was directed into the 40× objective of an Olympus BX 40 microscope (Olympus America Inc., Melville, NY) and onto the phage fiber through a cover glass which sealed the sample within a hygrostatic chamber. The backscattered (180°) Raman photons were collected with the same objective, passed through a notch filter, polarizing analyzer, and scrambler (Figure 1A), then directed onto the slit of a polychromator, and detected by a Peltier cooled, charge-coupled device detector (model Spectrum One; SPEX Inc., Edison, NJ).

The polarized Raman intensities I_{cc} and I_{cb} were measured by maintaining the fiber in a fixed orientation and rotating the polarizing analyzer (Figure 1A). These intensities correspond to the fiber tensor components *cc* and *cb*, respectively, where *c* is the fiber axis (also the virion axis) and *b* is perpendicular to *c*. The notation I_{cc} signifies that the electric vectors of both the exciting and scattered radiation are along *c*; similarly, I_{cb} signifies that the exciting and scattered electric vectors are along *c* and *b*, respectively. Subsequent rotation of the fiber by 90° on the microscope platform allowed I_{bb} and I_{bc} to be measured in succession using the same procedure as above. If the laser beam is precisely focused on the same portion of the sample throughout this protocol, then we expect $I_{cb} = I_{bc}$. This was found to be the case in nearly every experimental protocol. Occasionally, it was found that I_{cb} differed slightly from I_{bc}, indicating imprecise positioning. To correct for this effect, we defined the observed intensity ratio $(I_{bc})^{obs}/(I_{cb})^{obs} = 1 + \delta$, where $\delta \ll 1$, and the corrected intensity ratios $(I_{cc})^{cor} = (I_{cc})^{obs}(1 + \delta)$ and $(I_{bc})^{cor} = (I_{bc})^{obs}(1 + \delta)$. For convenience, we omit the superscript notations in all subsequent discussions and in the labeling of the figures shown below.

Data Analysis. Analysis of the polarized Raman intensities (I_{cc}, I_{bb}, I_{cb}, etc.) of a single Raman band requires interrelating two coordinate systems, *abc* and *xyz* (Figure 1B). The coordinate system *abc* is fixed on the cylindrically symmetric virus particle with *c* parallel to the virion axis and *a* and *b* equivalent and perpendicular to *c*, as shown in Figure 1B. The coordinate system *xyz* constitutes the set of principal axes of the Raman tensor associated with the given Raman band, which corresponds to a vibrational mode of a particular molecular subgroup. Because all subunits and therefore all identical molecular subgroups are arranged symmetrically with respect to *c*, the Raman tensor principal axes of the given Raman band are also arranged symmetrically with respect to *c*. Thus, the orientation of each axially symmetric *xyz* system can be expressed by two Eulerian angles, θ and χ, where θ is the angle between the *z* and *c* axes and χ is the angle between *y* and the line of intersection of the *xy* and *ab* planes. We seek to assign an appropriate *xyz* coordinate system to each Raman band of interest and then to determine the Eulerian angles, θ and χ, from the observed polarized Raman intensities, I_{cc}, I_{bb}, and I_{bc} (=I_{cb}).

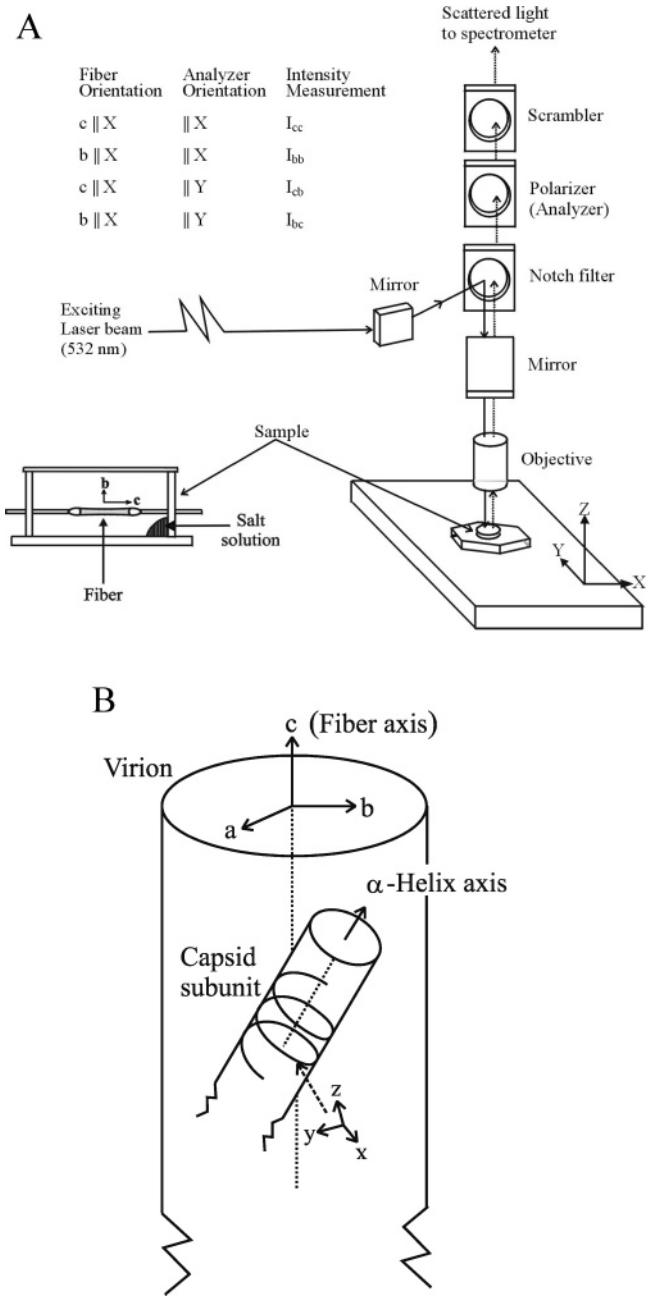

FIGURE 1: (A) Diagram of the Raman microscope and sample chamber, illustrating the coordinate systems defined for polarization of the laser electric vector (*XYZ*) and PH75 fiber (*abc*). Also indicated are the polarized Raman intensities (I_{cc}, I_{bb}, I_{cb}, I_{bc}) that correspond to the specific orientations of the fiber and incident and scattered electric vectors, as discussed in the text. (B) Schematic representation of the axis systems for an oriented fiber and a given Raman tensor. For each Raman band there corresponds a distinct Raman tensor principal axis system (*xyz*), which can be related to the *abc* axis system by an appropriate coordinate transformation (*7*, *10*).

The Raman tensor (α) corresponding to each Raman band is defined as the first derivative of the molecular polarizability with respect to the vibrational normal coordinate. Although α generally has six components, there are only three nonzero components in the *xyz* system, viz., α_{xx}, α_{yy}, and α_{zz}. Here, we consider only the relative magnitudes of these diagonal tensor components, $\alpha_{xx}/\alpha_{zz} = r_1$ and $\alpha_{yy}/\alpha_{zz} = r_2$. If these values are known, they can be related to the

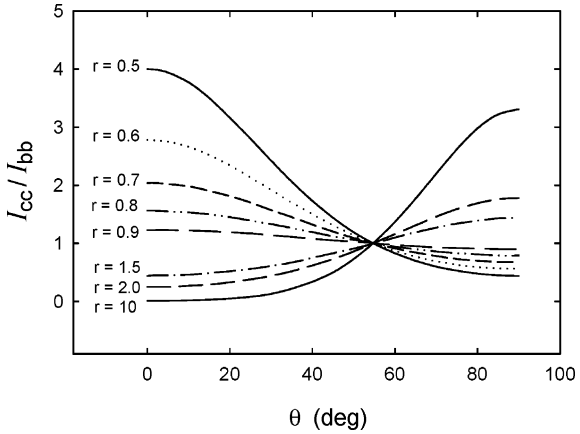

FIGURE 2: Dependence of the polarized Raman intensity ratio (I_{cc}/I_{bb}) on the angle of inclination (θ) of the subunit α-helix axis with respect to the virion axis for different values of the cylindrical Raman tensor ($r = \alpha_{xx}/\alpha_{zz} = \alpha_{yy}/\alpha_{zz}$). See also eq 3.

experimentally determined parameters I_{cc}/I_{bb} and I_{bc}/I_{bb} through the unknowns θ and χ by the equations:

$$I_{cc}/I_{bb} = 4[\sin^2\theta\,(r_1\cos^2\chi + r_2\sin^2\chi) + \cos^2\theta]^2/[\cos^2\theta\,(r_1\cos^2\chi + r_2\sin^2\chi) + r_1\sin^2\chi + r_2\cos^2\chi + \sin^2\theta]^2 \quad (1)$$

$$I_{bc}/I_{bb} = 2[\sin^2\theta\cos^2\theta\,(r_1\cos^2\chi + r_2\sin^2\chi - 1)^2 + \sin^2\theta\sin^2\chi\cos^2\chi^2\,(r_1 - r_2)^2]/[\cos^2\theta\,(r_1\cos^2\chi + r_2\sin^2\chi) + r_1\sin^2\chi + r_2\cos^2\chi + \sin^2\theta]^2 \quad (2)$$

Note that eqs 1 and 2 are based upon the customary assumption that the local vibration takes place in-phase for all equivalent atomic groups within each virion of the oriented fiber.

For a Raman band assignable to the peptide group of the subunit α-helix (such as the amide I mode at 1653 cm^{-1}), it is convenient to define the Raman tensor axes (*xyz*) so that *z* is parallel to the helix axis and *x* and *y* are perpendicular to *z*. Because of the cylindrical symmetry of the α-helix, *x* and *y* are equivalent. If the vibrational mode is totally symmetric (***A***-type symmetry species), then the *xyz* system also represents the tensor principal axes and the tensor has only the three nonzero components, α_{xx}, α_{yy}, and α_{zz}, where $\alpha_{xx} = \alpha_{yy}$. In this case $r_1 = r_2$ ($\equiv r$), and the polarized Raman intensity ratio I_{cc}/I_{bb} of eq 1 is reduced to eq 3, which allows determination of the inclination angle θ between the helix axis (*z*) and virion axis (*c*).

$$I_{cc}/I_{bb} = 4(r\sin^2\theta + \cos^2\theta)^2/(r\cos^2\theta + \sin^2\theta + r)^2 \quad (3)$$

The relationship between I_{cc}/I_{bb} and θ for various values of *r* is shown graphically in Figure 2. On the basis of the known Raman tensor of the peptide group and geometry of the α-helix, we have shown previously that for the amide I mode $r = 0.537$ (*7*). This *r* value is generally useful for estimating the average α-helix tilt angle (θ) in a biological assembly once the polarized Raman intensity ratio (I_{cc}/I_{bb}) has been measured. We note that if the amide I vibration takes place with either 100° or 200° phase difference between motions of adjacent peptide units (i.e., $\boldsymbol{E}_1$ or $\boldsymbol{E}_2$ symmetry species, respectively), the nonzero Raman tensor components

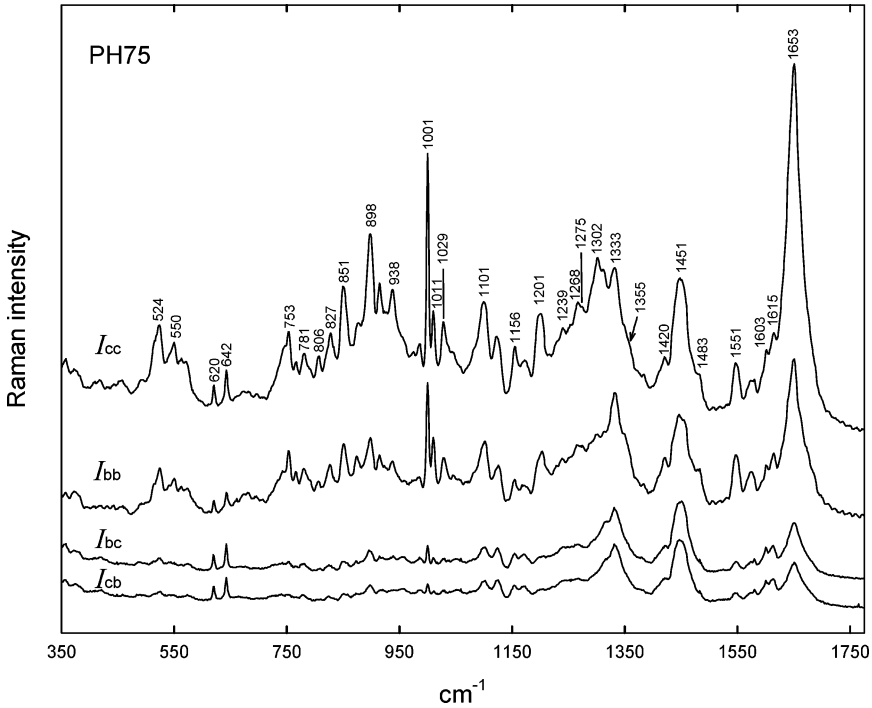

FIGURE 3: From top to bottom: Polarized I_{cc}, I_{bb}, I_{bc}, and I_{cb} Raman spectra (350−1750 cm^{-1}; 532 nm excitation) of an oriented fiber of PH75.

are respectively α_{xz} and α_{yz} or α_{xy}. In the former case, only I_{bc} and I_{cb} would be impacted, which does not affect eq 3; however, in the latter case, I_{bb} of eq 3 may be affected. Although we cannot directly assess the separate contributions to I_{bb} from the $\boldsymbol{A}$ and $\boldsymbol{E}_2$ modes, we assume that the $\boldsymbol{A}$ mode predominates and neglect the possible $\boldsymbol{E}_2$ contribution.

RESULTS AND INTERPRETATION

The I_{cc}, I_{bb}, I_{bc}, and I_{cb} polarized Raman spectra (532 nm excitation) obtained from an oriented fiber of the PH75 filamentous virus are shown in Figure 3. The I_{bc} and I_{cb} polarizations, as noted above (Materials and Methods), facilitate correction for polarization artifacts due to possible imprecision in the 90° rotation of the fiber with respect to the electric vector of the exciting radiation. The data of Figure 3 confirm the virtual identity of I_{bc} and I_{cb}. Table 1 lists the wavenumbers, I_{cc}/I_{bb} and I_{bc}/I_{bb} values, and assignments of all prominent bands in the polarized Raman spectra of PH75. More comprehensive Raman assignments based upon solution spectra have been given elsewhere (*3*). Structural insights from these results are discussed in the following sections.

Amide I of the α*-Helix.* Figure 3 shows that the peak of the amide I Raman band of PH75 is centered at 1653 cm^{-1}, which is a slightly higher wavenumber value than is observed for the amide I markers of fd (1650 cm^{-1}), Pf1 (1651 cm^{-1}), and Pf3 (1648 cm^{-1}) (*7*, *9*, *15*). This is consistent with the solution Raman results (*3*) and suggests either a perturbed α-helix or a minor nonhelical component to the overall subunit secondary structure. In the latter case, the data can be fit to a model comprising approximately 85% α-helix and 15% noncanonical helix (or nonhelical structure) (*3*). Thus, to a good approximation, the average peptide group of the PH75 capsid subunit can be considered α-helical. Figure 3 also shows that I_{cc}/I_{bb} for amide I is 2.5 ± 0.2, in contrast to 3.0 ± 0.1 for fd, Pf1, and Pf3 fibers (*7*, *9*, *15*). Together, these findings suggest a different average peptide group orientation angle (θ) for the capsid subunit of PH75 compared with the other filamentous virus subunits.

Because the amide I vibration (Figure 4, panel a) is localized within the peptide group and vibrational coupling among neighboring peptide groups is negligibly small, the contribution of an $\boldsymbol{E}_2$ mode can be ignored. Accordingly, for a helical subunit and with $r = 0.537$ (*12*), we find by eq 3 that $\theta = 25 \pm 5°$. Here, the error limit reflects the range of I_{cc}/I_{bb} values (2.5 ± 0.2) measured in successive experiments. A second potential source of error is imperfect alignment of filamentous virions within the fiber. A detailed analysis has shown, however, that this source of error is negligible in comparison to those involved in the experimental I_{cc} and I_{bb} measurements (*7*). Thus, the PH75 results can be interpreted as indicative of a larger average helix tilt angle (25 ± 5°) for PH75 than for other filamentous viruses (16 ± 4°). We note that to achieve for PH75 an average helix tilt angle of 16° would require a significantly larger amide I Raman tensor, i.e., $r = 0.600$ (see Figure 2) in lieu of the experimentally determined value of $r = 0.537$ (*12*). Finally, we note that the modestly lower polarization value ($I_{cc}/I_{bb} = 2.5$) observed for the amide I band of PH75 than for corresponding bands of fd, Pf1, and Pf3 ($I_{cc}/I_{bb} = 3.0$) is also consistent with the deviation of a small population of subunit residues from the canonical α-helix conformation. If it is assumed, for example, that a fraction (f) of PH75 subunit residues is oriented randomly and contributes $I_{cc}/I_{bb} \sim 1.0$ to the experimentally measured average of 2.5, while the canonical α-helix fraction $1 - f$ contributes $I_{cc}/I_{bb} = 3.0$, then $f \sim 0.25$. This is qualitatively consistent with the interpretation given previously for the solution Raman spectra of PH75 (*3*).

Amide III of the α*-Helix.* Amide III Raman markers of the α-helix, including those of fd, Pf1, and Pf3 (*16*), generally occur in the 1270−1300 cm^{-1} region, while those of nonhelical conformations occur in the 1230−1260 cm^{-1}

Table 1: Polarized Raman Frequencies, Intensities, and Assignments for PH75[a]

cm^{-1}	I	I_{cc}/I_{bb}	I_{bc}/I_{bb}	assignments
357	0.6	3.0	1.5	subunit main chain (α-helix)
374	0.4	1.0	0.4	subunit main chain (α-helix)
408	0.2	3.0	0	skeletal
420	0.3	2.7	0.9	subunit main chain (α-helix)
443	0.2	1.0	0	L, I
455	0.3	2.0	0	subunit main chain (α-helix)
493	0.4	1.8	0.9	V, G, thy, gua
524	2.1	1.7	0.18	amVI
550	1.6	2.0	0.2	V
563	1.2	1.8	0	I, V, L
570	1.1	1.8	0.3	
620	0.6	1.6	1.2	F
642	1.0	2.3	1.5	Y, M
662b	0.2	1.0	0	thy, gua
672b	0.3	1.0	0	thy
682b	0.3	1.0	0	gua
696b	0.2	1.0	0	M
746s	1.4	1.0	0.1	thy, I, L
753	1.8	1.6	0.2	W, A, F
766	0.9	0.9	0	amIV, W, thy, ade
781	1.1	1.2	0.2	cyt
791s	0.7	1.0	0.1	bk ν(OPO)
806	1.0	2.7	0.3	bk ν(OPO), W
827	1.5	1.6	0.3	Y, F, bk ν(OPO)
833s	1.1	1.0	0	bk ν(OPO)
851	2.8	1.92	0.21	Y, aliph
877	1.6	1.2	0.2	W, I, V
898	4.1	3.05	0.28	A, K
915	2.6	2.6	0.2	aliph
938	2.4	2.6	0.2	V, L
959s	1.0	1.0	0	V, L, K
975	0.5	2.0	0	I
986	0.7	2.0	0.5	I
1001	6.0	2.07	0.12	F
1011	1.6	1.16	0.26	W
1029	1.5	2.0	0.2	F
1045b	0.7	1.0	0	bk ν(CO)
1056b	0.3	1.3	0.7	F, bk ν(CO)
1082s	1.0	1.0	0.1	R, aliph
1101	2.4	1.88	0.24	A, aliph, bk $\nu(PO_2^-)$
1124	1.5	1.7	0.5	W, I, V, L
1156	1.3	2.3	0.6	W, I, V, L
1173b	0.9	1.8	1.0	Y, aliph
1201	2.3	2.1	0.08	W, F, Y
1216s	1.2	2.0	0	thy
1231s	1.5	1.0	0	V
1239	1.9	1.4	0.6	amIII, thy
1257s	2.0	2	0.5	amIII, cyt
1268	2.7	1.8	0.4	amIII
1275s	2.6	2.3	0.2	amIII, Y
1302	4.0	8.3	0.2	amIII, ade
1313	3.6	1.9	1	amIII, gua,
1333	3.7	0.7	0.4	W, ade, gua, aliph
1355	1.7	1.0	0	W
1384	0.8	1.0	0.3	gua, thy
1412s	1.0	1.0	0	bk $\delta(2'CH_2)$
1420	1.4	1.0	0.36	W, A, bk $\delta(2'CH_2)$
1451	3.6	1.7	1.0	sc $\delta(CH_2, CH_3)$, bk $\delta(5'CH_2)$
1464	1.6	1.18	0.74	sc $\delta(CH_2, CH_3)$, bk $\delta(5'CH_2)$
1483s	1.0	1.0	0.2	W, F, gua, ade
1551	1.4	0.97	0.16	W
1575	1.0	1.00	0.28	W, ade, gua
1581	1.0	1.0	1.0	W, F
1603s	1.9	1.25	1.0	F, Y
1615s	2.4	1.00	0.67	W, Y
1653	10	2.48	0.23	amI, thy

[a] Wavenumbers (cm^{-1} units), relative intensities (0−10 scale), and Raman polarization ratios are from Figure 3. Relative intensities are based upon an arbitrary value of 10 for the amide I marker at 1653 cm^{-1}. Assignments are based upon previous studies of model compounds and isotopomers (*16*, *26*−*28*). Single letter abbreviations are used for amino acids and three letter abbreviations for nucleotides. Other abbreviations: b, broad; s, shoulder; sc, side chain; aliph, aliphatic side chain; bk, DNA backbone; am, amide mode; δ, bond angle deformation; ν, bond stretching.

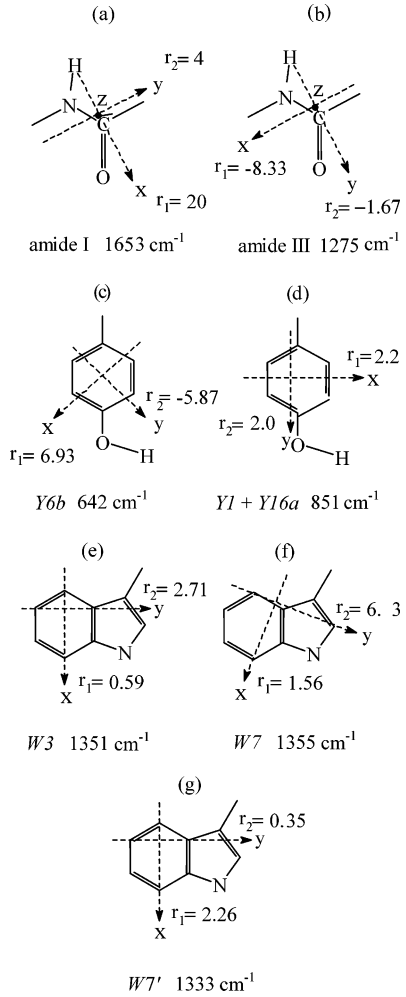

FIGURE 4: Raman scattering tensors associated with selected vibrational modes of the PH75 capsid subunit and DNA: (a) amide I, (b) amide III, (c) *Y6b* mode of Tyr, (d) *Y1* + *Y16a* mode of Tyr, (e) *W3* mode of Trp, (f) *W7* mode of Trp, and (g) *W7′* mode of Trp. In (a)−(g), *xyz* represents the principal axis system, $r_1 = \alpha_{xx}/\alpha_{zz}$, and $r_2 = \alpha_{yy}/\alpha_{zz}$, as defined in the text. Tensors (a) and (b) were determined from a polarized Raman analysis of aspartame single crystals (*12*). Tensors (c) and (d) were determined from a polarized Raman analysis of L-tyrosine single crystals (*14*). Tensors (e), (f), and (g) were determined from a polarized Raman analysis of *N*-acetyl-L-tryptophan single crystals (*13*).

region. Interestingly, for the PH75 fiber prominent peaks are observed near 1270 and 1240 cm^{-1} in the amide III region (Figure 3). A similar profile is observed for PH75 solutions (*3*). Thus, both the amide I and amide III profiles of PH75 imply a component of nonhelical secondary structure in the PH75 capsid subunit. This conclusion is consistent with the observation of a lower amide III polarized Raman intensity ratio ($I_{cc}/I_{bb} = 2.1 \pm 0.2$, Figure 3) for PH75 than observed for fd, Pf1, and Pf3 ($I_{cc}/I_{bb} \sim 3.0$) or predicted by eq 3 ($I_{cc}/I_{bb} = 3.6$).

Low-Frequency Modes of the α*-Helix.* The moderately intense Raman band of PH75 at 357 cm^{-1} (Figure 3) corresponds to the $\boldsymbol{E}_2/\boldsymbol{A}$ doublet of Pf1 at 336/351 cm^{-1}, which has been assigned to a main chain vibration of the subunit α-helix (*9*). The absence of doublet splitting and the higher wavenumber value in the case of PH75 suggest a larger vibrational force constant than for Pf1 and are consistent with less rigorous helical symmetry for PH75. The band at 455 cm^{-1} (Figure 3) is assigned to another main

Table 2: Raman Markers, Raman Polarizations, and Orientation Parameters of Trp Side Chains in Filamentous Viruses

virion residue		PH75 Trp 37	fd Trp 26	Pf3 Trp 38
W7′ mode	cm^{-1}	1333	1340	1335
	I_{cc}/I_{bb}	0.7 ± 0.1	0.4 ± 0.2	~0.5
W7 mode	cm^{-1}	1355	1364	1368
	I_{cc}/I_{bb}	1.0 ± 0.1	20 ± 5	7 ± 2
W3 mode	cm^{-1}	1551	1560	1548
	I_{cc}/I_{bb}	0.97 ± 0.05	2.8 ± 0.2	1.3 ± 0.3
Eulerian angle[a]	θ (deg)	45	74	77
	χ (deg)	59	61	45
torsion[b]	χ^1 (deg)	−118	−80	−84
	$\|\chi^{2,1}\|$ (deg)	95	120	93

[a] As shown in Figure 3 of ref *10* and defined by eq 1. [b] χ^1 is the dihedral angle relating the planes defined by Trp atoms N−C^{α}−C^{β} and C^{α}−C^{β}−C^{γ}; $\chi^{2,1}$ is the dihedral angle relating the planes defined by Trp atoms C^{α}−C^{β}−C^{γ} and C^{β}−C^{γ}−$C^{\delta 1}$.

chain vibration of the subunit α-helix, corresponding to the $\boldsymbol{E}_2/\boldsymbol{A}$ doublet of Pf1 at 435/445 cm^{-1}. Again, the higher wavenumber in PH75 than in Pf1 indicates a larger vibrational force constant. The strong band at 524 cm^{-1} (Figure 3), which is assigned to the amide VI vibration of the subunit α-helix (predominantly out-of-plane O═C−N−H bending), is similar in wavenumber and I_{cc}/I_{bb} intensity ratio (1.8) to its Pf1 counterpart.

In the case of Pf1 and fd virions, a Raman band assigned to the amide IV mode occurs in the 680−780 cm^{-1} interval (*17*). Overlapping Raman bands due to purine and pyrimidine ring vibrations of packaged DNA and to a ring vibration (*W18* mode) of the subunit tryptophan residue are also expected in this interval. For PH75 we observe a weak band near 766 cm^{-1} ($I_{cc}/I_{bb} < 1$), which may be due to overlapping contributions from amide IV as well as adenine and thymine residues of ssDNA. The intense band at 753 cm^{-1} is assigned to the *W18* mode of Trp 37.

Tryptophan Markers. Polarized Raman intensity ratios of the tryptophan markers at 1333 (*W7′* mode), 1355 (*W7*), and 1551 cm^{-1} (*W3*) and the wavenumber value of *W3* are useful for determining the precise orientation of the Trp 37 indolyl ring in PH75. The observed I_{cc}/I_{bb} values (Table 1 and Figure 3), which differ strikingly from those of the corresponding modes of Trp 26 in fd (*10*) and Trp 38 in Pf3 (*8*), clearly demonstrate a distinctive indolyl orientation for Trp 37 in the PH75 virion.

To obtain a first approximation to the Eulerian parameters (θ and χ, eq 1) defining the orientation of the indolyl plane with respect to the virion (fiber) axis, we use the I_{cc}/I_{bb} data summarized in the third column of Table 2 and the Raman tensors shown in Figure 4, panels e, f, and g, in conjunction with eq 1. Application of this procedure to Trp modes *W3*, *W7*, and *W7′* yields the contour lines in Figure 5. The contours converge within the relatively narrow region of θ,χ-space that is encircled near to the center of Figure 5. The radius of this circle takes into account the limits of error in the polarized Raman measurements (Table 2), from which we can conclude that the θ,χ-coordinates defining the indolyl plane orientation are within the limits $\theta = 40 \pm 7°$ and $\chi = 55 \pm 7°$. Use of the complementary I_{bc}/I_{bb} data for *W3* (Figure 3) with eq 2 provides additional support for this result. [Note that the use of a different set of Raman tensor principal axes for the *W7* mode (Figure 4, panel f) than for the *W3* and *W7′* modes (Figure 4, panels e and g) necessitates an appropriate coordinate transformation of the former prior to plotting the data in Figure 5. Further details of this graphical procedure have been described (*8*, *10*).

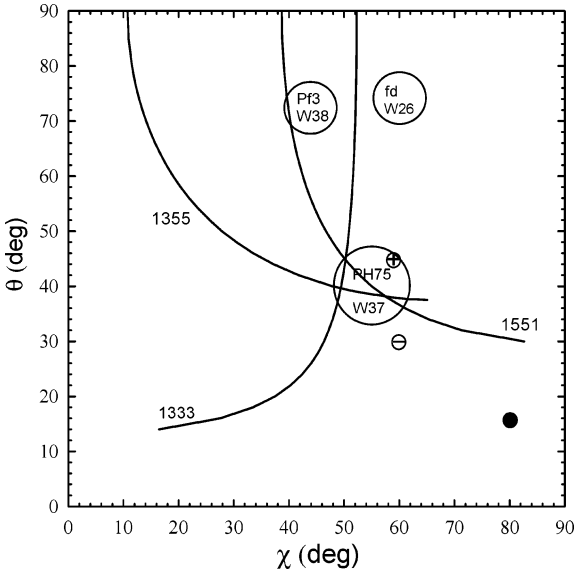

FIGURE 5: Contour maps in θ,χ-space showing I_{cc}/I_{bb} values for Trp 37 Raman markers at 1333, 1355, and 1551 cm^{-1}, as labeled. The large open circle near the center of the plot shows the region of θ,χ-space where data converge to a common set of θ,χ-coordinates, representing the Eulerian angles that define the orientation of the Trp 37 indolyl plane with respect to the virion axis. The radius of this circle, which is determined by experimental uncertainties in the data of Figure 3, fixes the coordinates to $\theta = 40 \pm 7°$ and $\chi = 55 \pm 7°$. The complementary I_{bc}/I_{bb} value measured for the 1551 cm^{-1} marker (not shown) also falls within this circle. Additional supporting data (see text) allow refinement of the coordinates to $\theta = 45°$ and $\chi = 59°$ (symbol ⊕). Circles representing the θ,χ-coordinates determined previously by polarized Raman spectroscopy for Trp 26 of fd (*10*) and Trp 38 of Pf3 (*8*) are also shown for comparison. The Trp 37 θ,χ-coordinates proposed previously on the basis of model building studies (*1*) are indicated by the filled circle (●). The θ,χ-coordinates (30°,60°), which were computed for Trp 37 on the basis of a negatively signed value of $\chi^{2,1}$ and do not satisfactorily fit the experimental data, are indicated by the encircled minus sign (see text).

Finally, the above results on θ and χ can be further refined using additional constraints imposed on the Trp 37 side chain torsion angles χ^1 (N−C^{α}−C^{β}−C^{γ}) and $\chi^{2,1}$ (C^{α}−C^{β}−C^{γ}−$C^{\delta 1}$). In the case of χ^1 we rely on the protein database of Ponder and Richards (*18*) and fiber diffraction-based model building studies of other filamentous viruses, suggesting values in the range $-70° > \chi^1 > -125°$ (*19*, *20*). In the case of $\chi^{2,1}$, we use the empirical correlation based upon *W3* (*21*), requiring $|\chi^{2,1}| = 95°$ and the results of ROA data suggesting that the sign of $\chi^{2,1}$ is negative (*2*). Thus, the optimal values of χ^1 and $\chi^{2,1}$ that we find consistent with the data of Figure 5 are −118° and +95°, respectively. These place θ and χ at 45° and 59°, respectively, as indicated by the encircled plus symbol (⊕) in Figure 5. Interestingly, the alternative sign for the $\chi^{2,1}$ torsion angle (−95°, indicated by the encircled minus symbol in Figure 5) does not provide a satisfactory fit to the polarized Raman data, despite recent speculation in this regard (*2*). Also for comparison, we have labeled Figure 5 to show the θ,χ-coordinates determined previously for Trp 26 of fd (*10*) and Trp 38 of Pf3 (*8*).

Atomic coordinates proposed here for the PH75 subunit structure in the vicinity of the Trp 37 side chain are given

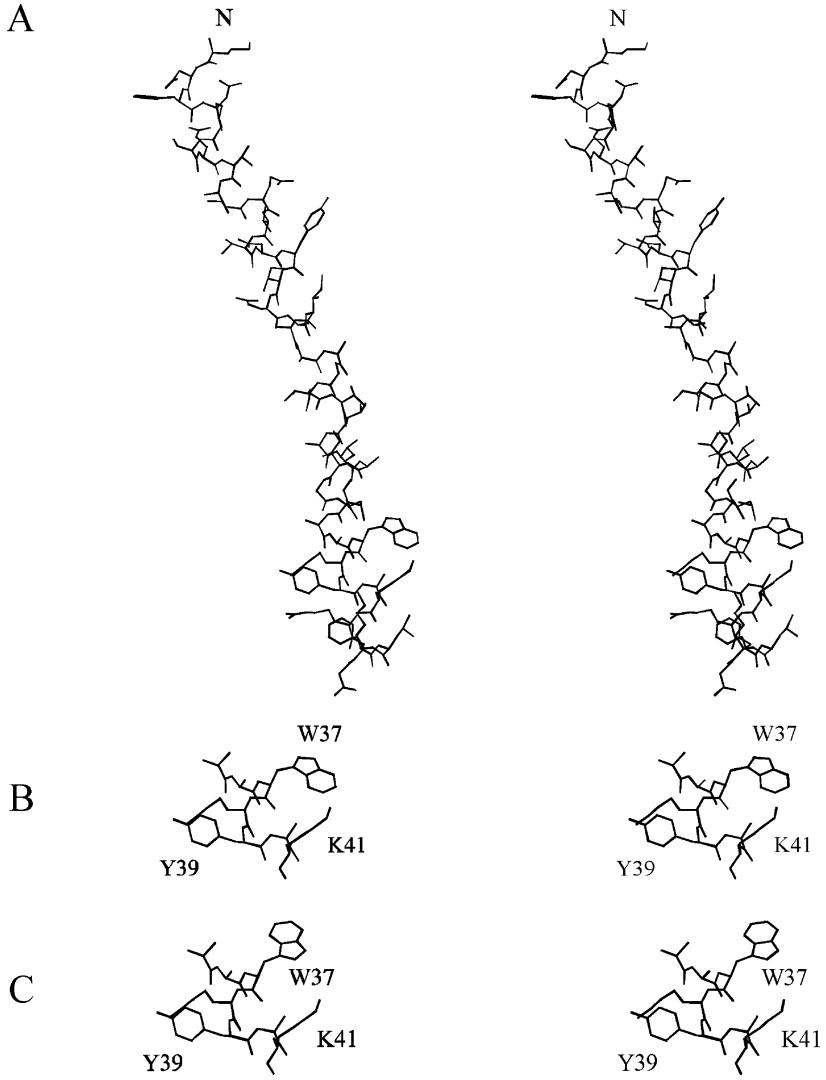

FIGURE 6: (A) Stereo molecular model of the PH75 capsid subunit incorporating values of (45°,59°) for the (θ,χ)-pair. Other coordinates are from PDB entry 1HGZ (*1*). (B) Stereoview of the C-terminal region (residues 35−41). This view shows the proximities of the indole ring of Trp 37 to the $N^{\zeta}H_3^+$ group of Lys 41 and of the phenolic ring of Tyr 39 to the $N^{\zeta}H_3^+$ group of Lys 38, reminiscent of cation−π interactions (*29*). (C) Stereoview of the C-terminal region (residues 35−41) assuming the alternative (negative) sign for $\chi^{2,1}$ (see text).

Table 3: Atomic Coordinates of the Trp 37 Side Chain in the PH75 Capsid Subunit Determined by Polarized Raman Spectroscopy[a]

atom				Cartesian (and fiber axis) coordinates		
				x (*a*)	*y* (*b*)	*z* (*c*)
11	N	Trp A	37	−11.681	−13.181	−8.014
12	CA	Trp A	37	−12.298	−11.943	−8.283
13	C	Trp A	37	−11.445	−11.243	−9.368
14	O	Trp A	37	−11.984	−10.604	−10.268
15	CB	Trp A	37	−12.489	−11.091	−7.004
16	CG	Trp A	37	−13.924	−10.803	−6.736
17	CD1	Trp A	37	−14.758	−11.496	−5.907
18	CD2	Trp A	37	−14.730	−9.849	−7.421
19	NE1	Trp A	37	−16.023	−10.991	−5.998
20	CE2	Trp A	37	−16.027	−9.976	−6.922
21	CE3	Trp A	37	−14.466	−8.886	−8.416
22	CZ2	Trp A	37	−17.067	−9.180	−7.389
23	CZ3	Trp A	37	−15.500	−8.104	−8.889
24	CH2	Trp A	37	−16.787	−8.255	−8.373

[a] Atom nomenclature and the Cartesian coordinate system (*xyz*) follow those of PDB entry 1HGZ. The fiber axis coordinate system (*abc*) is also indicated.

in Table 3. A corresponding stereo model is shown in Figure 6, panels A and B. This structure represents a significant revision to the Trp 37 orientation in the model proposed previously by Marvin and co-workers (Protein Data Bank entry 1HGZ) (*1*), as can be seen by noting the significantly different θ,χ-coordinates for the indolyl plane in the 1HGZ structure (● symbol in Figure 5).

Tyrosine Markers. The two tyrosines of the PH75 subunit (Tyr 15 and Tyr 39) exhibit several prominent Raman markers (Table 1). Those for which reliable Raman tensors are available include the highly polarized bands at 642 cm^{-1} (I_{cc}/I_{bb} = 2.0) and 851 cm^{-1} (I_{cc}/I_{bb} = 1.9). The observed I_{cc}/I_{bb} values are quite similar to those of the corresponding tyrosine Raman markers (Tyr 25 and Tyr 40) in Pf1 (*9*), which indicates similar average orientations (θ,χ-coordinates) for the two tyrosines in both PH75 and Pf1. In particular, using the tensors of Figure 4, panels c and d, we obtain average Eulerian angles of $\theta = 80 \pm 5°$ and $\chi = 33 \pm 5°$ for Tyr 15 and Tyr 39 of PH75, compared with $\theta = 76 \pm 10°$ and $\chi = 34 \pm 10°$ for Tyr 25 and Tyr 40 of Pf1 (*9*). Interestingly, very similar results were also obtained for the average Tyr 21 and Tyr 24 orientations in fd, for which $\theta = 71 \pm 5°$ and $\chi = 36 \pm 5°$ (*11*). (In the case of fd, the availability of single-site mutants Y21M and Y24M also

permitted demonstration of virtually identical side chain orientation for the Tyr 21 and Tyr 24 side chains individually.)

We note that, as reported previously for solution Raman spectra of PH75 (*3*), the fiber spectra of Figure 3 clearly confirm the presence of both components of the 851/827 cm^{-1} Fermi doublet. The data are quantitatively consistent with hydrogen bonding by one tyrosine phenoxyl and sequestering of the other from hydrogen-bonding interaction. Thus, although the tyrosine pairs in subunits of fd, Pf1, and PH75 are engaged in very different hydrogen-bonding states (*9*, *22*), all adopt nearly the same ring orientations. Such a highly conserved structural feature may reflect an intersubunit packing scheme common to each of the virions so far investigated. The apparently conserved tyrosine orientation among three different filamentous virions contrasts strikingly with the distinctive tryptophan orientations noted above for PH75, Pf1, and fd (Figure 5).

Phenylalanine Markers. Residues Phe 3 and Phe 43 of the PH75 subunit generate prominent phenyl ring markers at 620, 1001, and 1029 cm^{-1} with respective I_{cc}/I_{bb} values of 1.6, 2.07, and 2.0. Because the Raman tensors for these phenyl ring markers are not known, the average phenyl ring orientation for Phe 3 and Phe 43 cannot be calculated. However, such high polarizations suggest that the tensor axis of the lowest polarizability component (i.e., the axis perpendicular to the plane of the phenyl ring) is likely oriented close to normal to the virion axis (*c*). This would place the average phenyl ring plane close to parallel to the virion axis.

The relatively large I_{cc}/I_{bb} values observed for Phe markers of PH75 contrast sharply with the cases of fd and Pf3, for which the corresponding Phe markers all exhibit $I_{cc}/I_{bb} \sim 1$. Again, although quantitative assessments of the θ,χ-coordinates are not possible, the orientation of the average phenyl ring in both the fd subunit (residues Phe 11, Phe 42, and Phe 45) and Pf3 subunit (Phe 43 and Phe 44) is very different from that of PH75. An I_{cc}/I_{bb} value close to 1 implies that in both fd and Pf3 the average Phe ring is either unordered or oriented at the magic angle (∼54°).

DNA Markers. For the Pf1 virus, prominent Raman bands of the deoxynucleotide residues of packaged ssDNA occur at 680 (dG), 720 (dA), 750 (dT), and 782 cm^{-1} (dC). All are due to ring breathing vibrations of the base residues (*9*, *23*), and all exhibit significant Raman polarization effects, i.e., values of $I_{cc}/I_{bb} > 1$. For PH75, on the other hand, corresponding DNA markers (∼682, ∼725, ∼745, and ∼780 cm^{-1}) are much less prominent (Figure 3) and lack Raman polarization effects ($I_{cc}/I_{bb} \sim 1$). This is similar to the situation encountered for fd and can be attributed to efficient stacking and significant tilting of the bases in the packaged DNAs of PH75 and fd in contrast to essentially unstacked and unidirectionally oriented bases in the packaged DNA of Pf1 (*9*, *24*). The absence of a preferred orientation of bases in packaged PH75 DNA is also consistent with the observation that for the above-noted DNA markers $I_{bc}/I_{bb} \sim 0$. The deoxynucleoside conformations indicated by the Raman markers of packaged PH75 DNA have been further discussed elsewhere (*3*).

DISCUSSION

Fiber X-ray diffraction patterns reported for PH75 (*1*) and Pf1 (*25*) are very similar to one another in their central portions, with respect to both layer line positions and intensity distributions. Significant differences are observed, however, in the outer portions of the electron density map. The diffraction results indicate a similar capsid symmetry ($\boldsymbol{C}_1\boldsymbol{S}_{5.4}$ or class II) and subunit shape (predominantly α-helical) but suggest different structural details at the side chain level and subunit/DNA interface. Some of these differences have been elucidated in the present polarized Raman analysis.

First, it is evident that the electronic structure as well as the geometry of the average peptide group in subunits of PH75 (∼80% α-helix) and Pf1 (∼100% α-helix) must be significantly different, despite the similar arrangement of subunits in the two viral capsids. This is evidenced not only by the different amide I peak positions, band shapes, and polarizations in the two virions but also by the different amide III and amide IV band polarizations and different $\boldsymbol{E}_2/\boldsymbol{A}$ splittings observed for low-frequency helix modes. All of these differences point to less uniformity of α-helical secondary structure in the PH75 subunit than in Pf1. The distinctive secondary structure of the PH75 subunit may confer greater thermostability to the viral capsid for assembly and viability of the thermophilic host at 70 °C.

We have found an orientation for the tryptophan (Trp 37) side chain of the PH75 subunit that distinguishes it markedly from Trp 26 of fd and Trp 38 of Pf3. In the case of PH75, the plane of the indolyl ring projects close to equatorially from the α-helix axis and is positioned outwardly from the α-helix surface (Figure 6A), whereas for both fd and Pf3 the indolyl ring planes are aligned closer to axially and are accommodated nearer to the subunit surface (*8*, *10*). The indole ring orientation in PH75 (Figure 6) may be required for specific intrasubunit and/or intersubunit interactions that confer added thermostability to the virion assembly. Conversely, the tyrosines of PH75 (Tyr 15 and Tyr 39) exhibit phenolic ring orientations that are similar to the tyrosines of fd (Tyr 21 and Tyr 24) and Pf1 (Tyr 25 and Tyr 40). Nevertheless, the pair of PH75 tyrosines is unique by virtue of the participation of one phenoxyl in hydrogen-bonding interaction. Such interaction may also contribute to intrasubunit and intersubunit contacts that confer added thermostability to the PH75 assembly.

Recently, Blanch and co-workers noted that, among several proteins investigated by ROA, the sign of the *W3* ROA band ca. 1550 cm^{-1} is positive when $\chi^{2,1} > 0$ and negative when $\chi^{2,1} < 0$ (*2*). These investigators proposed that the sign of the *W3* ROA band may correlate through a sin $\chi^{2,1}$ relationship. This does not appear to be the case, however, for Trp 37 of PH75. Despite its negative *W3* ROA band, the value $\chi^{2,1} = -95°$ does not provide satisfactory agreement with the polarized Raman results, as seen in Figure 5. A value of $-95°$ for $\chi^{2,1}$ would also position the indole moiety of Trp 37 away from the charged side chain terminus of Lys 41 (Figure 6C), thus preventing an orientation that would appear to be more favorable to intrasubunit cation$-\pi$ interaction (cf. Figure 6, panels B and C).

Finally, in contrast to the rather regular arrangement of deoxynucleotide residues indicated by polarized Raman measurements on packaged Pf1 and Pf3 DNAs (*9*, *15*), we find evidence for less uniformity in the deoxynucleotide orientations of packaged PH75 DNA. The present results show that nucleotides along the DNA chain do not have base planes oriented unidirectionally with respect to the virion

axis, which suggests that the genome of PH75 may be more highly condensed within the nucleocapsid than corresponding genomes of Pf1 and Pf3. More detailed discussion of structural distinctions between PH75 and filamentous phages infecting mesophilic hosts (fd, Pf1, Pf3) has been given elsewhere (*3*).

ACKNOWLEDGMENT

We thank our colleague Dr. Stacy A. Overman for many helpful suggestions to improve the manuscript and for assistance in the preparation of Table 1 and Figure 6.

REFERENCES

1. Pederson, D. M., Welsh, L. C., Marvin, D. A., Sampson, M., Perham, R. N., Yu, M., and Slater, M. R. (2001) The protein capsid of filamentous bacteriophage PH75 from *Thermus thermophilus*, *J. Mol. Biol. 309*, 401−421.
2. Blanch, E. W., Hecht, L., Day, L. A., Pederson, D. M., and Barron, L. D. (2001) Tryptophan absolute stereochemistry in viral coat proteins from Raman optical activity, *J. Am. Chem. Soc. 123*, 4863−4864.
3. Overman, S. A., Bondre, P., Maiti, N. C., and Thomas, G. J., Jr. (2004) Structural characterization of the filamentous bacteriophage PH75 from *Thermus thermophilus* by Raman and UV-resonance Raman spectroscopy, *Biochemistry 43*, 13129−13136.
4. Day, L. A., Marzec, C. J., Reisberg, S. A., and Casadevall, A. (1988) DNA packing in filamentous bacteriophages, *Annu. Rev. Biophys. Biophys. Chem. 17*, 509−539.
5. Marvin, D. A. (1998) Filamentous phage structure, infection and assembly, *Curr. Opin. Struct. Biol. 8*, 150−158.
6. Tsuboi, M., and Thomas, G. J., Jr. (1997) Raman scattering tensors in biological molecules and their assemblies, *Appl. Spectrosc. Rev. 32*, 263−299.
7. Overman, S. A., Tsuboi, M., and Thomas, G. J., Jr. (1996) Subunit orientation in the filamentous virus Ff (fd, f1, M13), *J. Mol. Biol. 259*, 331−336.
8. Tsuboi, M., Overman, S. A., Nakamura, K., Rodriguez-Casado, A., and Thomas, G. J., Jr. (2003) Orientation and interactions of an essential tryptophan (Trp-38) in the capsid subunit of Pf3 filamentous virus, *Biophys. J. 84*, 1969−1976.
9. Tsuboi, M., Kubo, Y., Ikeda, T., Overman, S. A., Osman, O., and Thomas, G. J., Jr. (2003) Protein and DNA residue orientations in the filamentous virus Pf1 determined by polarized Raman and polarized FTIR spectroscopy, *Biochemistry 42*, 940−950.
10. Tsuboi, M., Overman, S. A., and Thomas, G. J., Jr. (1996) Orientation of tryptophan-26 in coat protein subunits of the filamentous virus Ff by polarized Raman microspectroscopy, *Biochemistry 35*, 10403−10410.
11. Tsuboi, M., Ushizawa, K., Nakamura, K., Benevides, J. M., Overman, S. A., and Thomas, G. J., Jr. (2001) Orientations of Tyr 21 and Tyr 24 in the capsid of filamentous virus Ff determined by polarized Raman spectroscopy, *Biochemistry 40*, 1238−1247.
12. Tsuboi, M., Ikeda, T., and Ueda, T. (1991) Raman microscopy of a small uniaxial crystal: Tetragonal aspartame, *J. Raman Spectrosc. 22*, 619−626.
13. Tsuboi, M., Ueda, T., Ushizawa, K., Ezaki, Y., Overman, S. A., and Thomas, G. J., Jr. (1996) Raman tensors for the tryptophan side chain in proteins determined by polarized Raman microspectroscopy of oriented *N*-acetyl-L-tryptophan crystals, *J. Mol. Struct. 379*, 43−50.
14. Tsuboi, M., Ezaki, Y., Aida, M., Suzuki, M., Yimit, A., Ushizawa, K., and Ueda, T. (1998) Raman scattering tensors of tyrosine, *Biospectroscopy 4*, 61−71.
15. Wen, Z. Q., Overman, S. A., Bondre, P., and Thomas, G. J., Jr. (2001) Structure and organization of bacteriophage Pf3 probed by Raman and ultraviolet resonance Raman spectroscopy, *Biochemistry 40*, 449−458.
16. Thomas, G. J., Jr., Prescott, B., and Day, L. A. (1983) Structure similarity, difference and variability in the filamentous viruses fd, If1, IKe, Pf1, Xf and Pf3, *J. Mol. Biol. 165*, 321−356.
17. Overman, S. A., and Thomas, G. J., Jr. (1998) Amide modes of the α-helix: Raman spectroscopy of filamentous virus fd containing peptide ^{13}C and ^{2}H labels in coat protein subunits, *Biochemistry 37*, 5654−5665.
18. Ponder, J. W., and Richards, F. M. (1987) Tertiary templates for proteins. Use of packing criteria in the enumeration of allowed sequences for different structural classes, *J. Mol. Biol. 193*, 775−791.
19. Marvin, D. A., Hale, R. D., Nave, C., and Citterich, M. H. (1994) Molecular models and structural comparisons of native and mutant class I filamentous bacteriophages: Ff (fd, f1, M13), If1 and IKe, *J. Mol. Biol. 235*, 260−286.
20. Symmons, M. F., Welsh, L. C., Nave, C., Marvin, D. A., and Perham, R. N. (1995) Matching electrostatic charge between DNA and coat protein in filamentous bacteriophage. Fibre diffraction of charge-deletion mutants, *J. Mol. Biol. 245*, 86−91.
21. Miura, T., Takeuchi, H., and Harada, I. (1989) Tryptophan Raman bands sensitive to hydrogen bonding and side-chain conformation, *J. Raman Spectrosc. 20*, 667−671.
22. Arp, Z., Autrey, D., Laane, J., Overman, S. A., and Thomas, G. J., Jr. (2001) Tyrosine Raman signatures of the filamentous virus Ff are diagnostic of non-hydrogen-bonded phenoxyls: Demonstration by Raman and infrared spectroscopy of *p*-cresol vapor, *Biochemistry 40*, 2522−2529.
23. Thomas, G. J., Jr., Prescott, B., Opella, S. J., and Day, L. A. (1988) Sugar pucker and phosphodiester conformations in viral genomes of filamentous bacteriophages: fd, If1, IKe, Pf1, Xf, and Pf3, *Biochemistry 27*, 4350−4357.
24. Wen, Z. Q., Armstrong, A., and Thomas, G. J., Jr. (1999) Demonstration by ultraviolet resonance Raman spectroscopy of differences in DNA organization and interactions in filamentous viruses Pf1 and fd, *Biochemistry 38*, 3148−3156.
25. Welsh, L. C., Symmons, M. F., and Marvin, D. A. (2000) The molecular structure and structural transition of the α-helical capsid in filamentous bacteriophage Pf1, *Acta Crystallogr., Sect. D: Biol. Crystallogr. 56* (Part 2), 137−150.
26. Aubrey, K. L., and Thomas, G. J., Jr. (1991) Raman spectroscopy of filamentous bacteriophage Ff (fd, M13, f1) incorporating specifically-deuterated alanine and tryptophan side chains: Assignments and structural interpretation, *Biophys. J. 61*, 1337−1349.
27. Overman, S. A., and Thomas, G. J., Jr. (1995) Raman spectroscopy of the filamentous virus Ff (fd, fl, M13): Structural interpretation for coat protein aromatics, *Biochemistry 34*, 5440−5451.
28. Overman, S. A., and Thomas, G. J., Jr. (1999) Raman markers of nonaromatic side chains in an α-helix assembly: Ala, Asp, Glu, Gly, Ile, Leu, Lys, Ser, and Val residues of phage *fd* Subunits, *Biochemistry 38*, 4018−4027.
29. Ma, J. C., and Dougherty, D. A. (1997) The cation-π interaction, *Chem. Rev. 97*, 1303−1324.

BI0479306